Insertases Scramble Lipids: Molecular Simulations of MTCH2

Ladislav Bartoš,[†,‡] Anant K. Menon,[¶] and Robert Vácha[*,†,§,‡]

†*CEITEC – Central European Institute of Technology, Masaryk University, Kamenice 753/5, 625 00 Brno, Czech Republic*
‡*National Centre for Biomolecular Research, Faculty of Science, Masaryk University, Kamenice 5, 625 00 Brno, Czech Republic*
¶*Department of Biochemistry, Weill Cornell Medical College; New York, NY 10065, USA*
§*Department of Condensed Matter Physics, Faculty of Science, Masaryk University, Kotlářská 267/2, 611 37 Brno, Czech Republic*

E-mail: robert.vacha@muni.cz

Abstract

Scramblases play a pivotal role in facilitating bidirectional lipid transport across cell membranes, thereby influencing lipid metabolism, membrane homeostasis, and cellular signaling. MTCH2, a mitochondrial outer membrane protein insertase, has a membrane-spanning hydrophilic groove resembling those that form the lipid transit pathway in known scramblases. Employing both coarse-grained and atomistic molecular dynamics simulations, we now show that MTCH2 significantly reduces the free energy barrier for lipid movement along the groove and therefore can indeed function as a scramblase. Notably, the scrambling rate of MTCH2 in silico is similar to that of VDAC, a recently discovered scramblase of the outer mitochondrial membrane, suggesting a potential complementary physiological role for these mitochondrial proteins. Finally, our findings suggest that other insertases which possess a hydrophilic path across the membrane like MTCH2, can also function as scramblases.

TOC Graphic

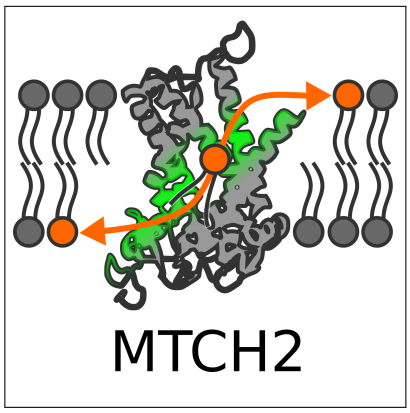

Keywords

scramblase | insertase | molecular dynamics | flip-flop rate | free energy barrier | hydrophilic groove | membrane defect

The spontaneous movement of polar lipids from one side of a membrane bilayer to the other is slow and is accelerated in cells to a physiologically relevant rate by lipid transporters[14,15]. Flippases and floppases are transporters which move lipids unidirectionally, against their concentration gradient in an ATP-dependent manner, whereas scramblases enable bidirectional lipid movement without input of metabolic energy. Scramblases typically possess transmembrane helices that are not fully hydrophobic – these helices form a membrane-spanning hydrophilic groove through which phospholipids can move in analogy to a credit card (phospholipid) being swiped through a card reader (scramblase)[14]. Known scramblases are alpha-helical proteins[7,8,13,18], but recently, a beta-barrel scramblase, the voltage-dependent anion channel (VDAC), was identified[5]. The VDAC barrel has membrane-facing polar residues that, when paired with the same residues in a second beta barrel at a dimer interface, create a local membrane defect along which lipids cross the membrane in credit card mode. Therefore, the presence or ability to form a hydrophilic groove across the membrane seems to be a common feature for lipid scrambling.

Insertases assist in the integration of membrane proteins into lipid bilayers[9]. Their activity is necessary because membrane proteins typically have hydrophilic segments that do not spontaneously translocate across the membrane. The translocating moieties of these proteins are thus amphiphilic, similar to lipids, and it is interesting to consider whether insertases and scramblases may share a common mechanism even though lipids and their polar headgroups are generally smaller than the translocating parts of membrane proteins.

Recent work demonstrated that the mitochondrial outer membrane protein MTCH2 is an insertase[3]. MTCH2 has a wide transbilayer groove lined with polar and charged residues, reminiscent of the hydrophilic grooves of scramblases, leading us to hypothesize that it may function as a scramblase. To test this hypothesis, we performed coarse-grained and atomistic molecular dynamics (MD) simulations of MTCH2 in a model lipid bilayer. We used a MTCH2 structure predicted by AlphaFold[6,17] and simulated it in 1-palmitoyl-2-oleoyl-sn-glycero-3-phosphocholine (POPC) membrane.

We started with coarse-grained simulations using the Martini 3 force field[16]. We conducted three unbiased simulations (each of 10 µs), to analyze the spontaneous scrambling activity of MTCH2. Additionally, we calculated the free energy of lipid flip-flop along the MTCH2 groove and compared it with the free energy of flip-flop in a protein-free POPC membrane.

In the unbiased simulations with MTCH2, we observed rapid insertion of lipids from the upper leaflet into the cavity of MTCH2 (see Figure 1 A-B). The cavity of MTCH2 is situated between α-helices 1 (residues 1–31), 3 (residues 74–100), 4 (residues 117–151), 6 (residues 182–207), and 7 (residues 216–247). It is shaped like a funnel that opens towards the leaflet with the N-terminus and is lined with a large number of hydrophilic and charged amino acid sidechains (see Figure 1 B). This cavity has already been described as the structural basis of the insertase activity of MTCH2 by Guna et al[3].

In our Martini 3 simulations, the insertion of lipids into the cavity was quickly followed by a large number of flip-flop events during which lipids traversed between the membrane leaflets in both directions (see Figure 2 A Left). We identified a mostly hydrophilic pathway extending the cavity towards the opposite leaflet (with C-terminus) and allowing lipids to pass along MTCH2 through the entire hydrophobic membrane core. This extended hydrophilic pathway (further called "C-terminal pathway") starts with Y235 located in helix 7 near the bottom of the cavity and continues with N282, S283, S279, K287, and N277 until the phosphate level of the lower membrane leaflet is reached. The entry into this pathway is however partly obstructed by several hydrophobic residues, namely F228, M232 (α-helix 7) and L284, F285, and F286 (all located in a C-terminal loop following α-helix 8). See Figure 1 C for a more detailed view of the C-terminal pathway and the "hydrophobic gate".

To further support our qualitative observations and demonstrate local membrane de-

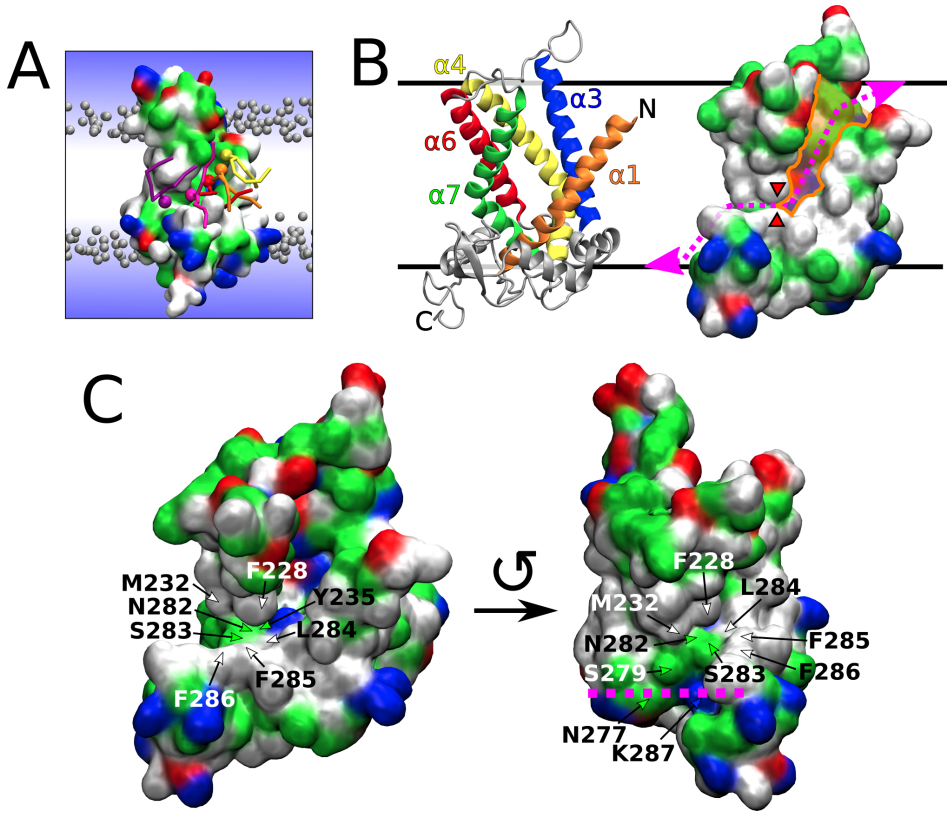

Figure 1: A) Snapshot from a Martini 3 simulation showing several lipids (colored in yellow, orange, red, magenta, and purple) translocating along the scrambling pathway of MTCH2. The protein is shown as a molecular surface colored according to the character of its residues (hydrophilic = green, hydrophobic = white, positively charged = blue, negatively charged = red). Bulk lipids are depicted as gray beads (phosphate groups) with hydrophobic tails omitted for clarity. Water is represented only schematically as a blue gradient, omitting the presence of water in the cavity of the protein for visual clarity. B) Two visualisations of the atomistic structure of MTCH2 after 3 µs of atomistic simulation. Left. Cartoon representation showing α-helices forming the cavity of the protein. Right. Molecular surface representation showing the cavity (colored in orange), the scrambling pathway (dotted magenta line) and the position of the "hydrophobic gate" (red wedges). C) More detailed views of the atomistic structure of MTCH2 showing residues of the C-terminal pathway and the "hydrophobic gate". The structure on the left depicts the frontal and slightly superior view of the MTCH2 cavity. The structure on the right shows MTCH2 rotated counterclockwise by roughly 90° showing frontal view of the C-terminal pathway, while the cavity is mostly hidden. Purple line shows the approximate position of the lipid headgroups in the lower leaflet. The top of the figure represents the cytosol, and the bottom represents the intermembrane space of mitochondria.

fect/thinning, we calculated the density of phosphates and the density of water around MTCH2 in all three unbiased simulations. As shown in Figure 2 B Left, the density of phosphates is significantly increased in the cavity of the protein as well as in the C-terminal pathway indicating that phosphates readily pass through the membrane along MTCH2. Similarly, Figure 2 C Left shows the increased density of water in the cavity of MTCH2. Unlike phosphates, water density was reduced (but not absent) along the C-terminal pathway.

The identified features of MTCH2, including the hydrophilic pathway, water defect, and membrane disruption, align with those observed in other scramblases, such as TMEM16[1,7], opsin[8,12], and VDAC[5]. Notably, MTCH2 shares with the other scramblases the

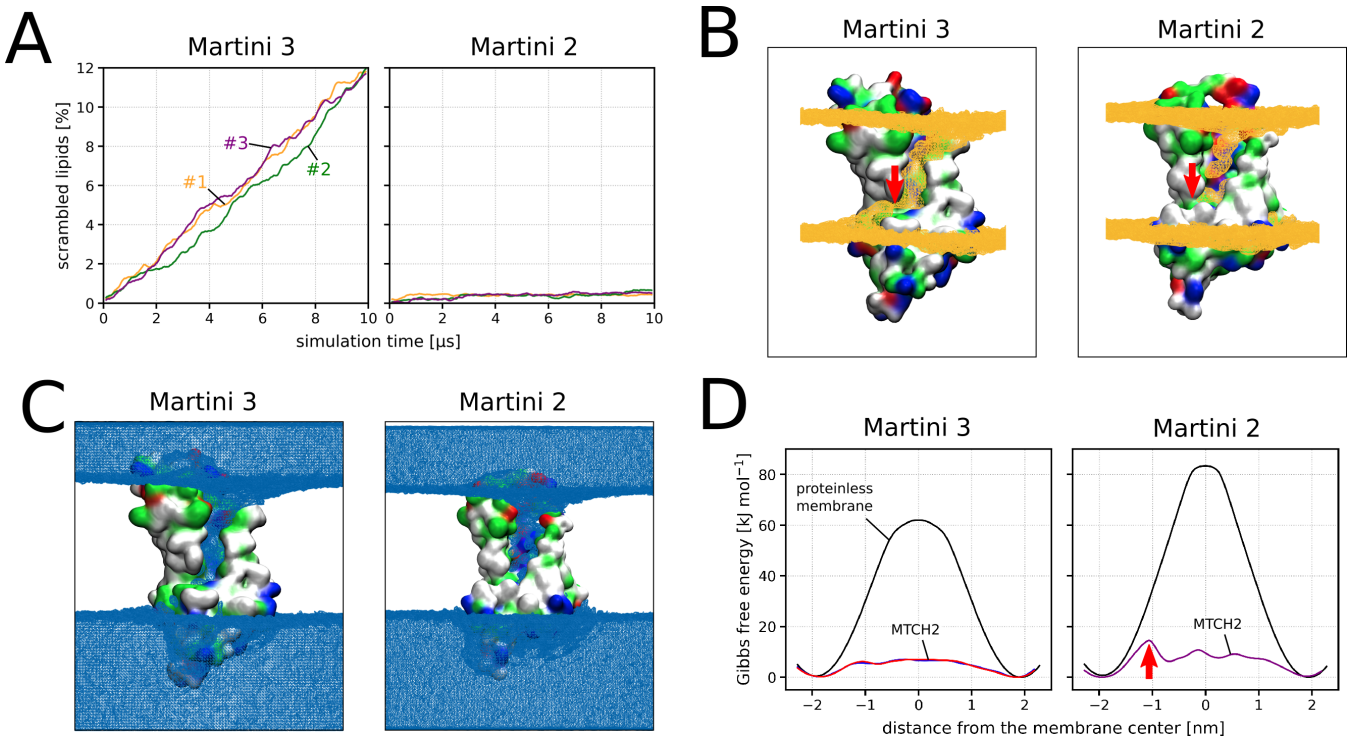

Figure 2: Comparison of Martini 3 and Martini 2 simulations. A) Scrambling rate of MTCH2 in a POPC membrane shown as the percentage of "scrambled lipids" in time (running average over 200 ns). Each line corresponds to single 10 µs long Martini simulation. Lipid was considered to be scrambled when it was located in the opposite leaflet to its original one. Scrambling rate of lipids in a pure POPC membrane is zero in both models (on the simulated time scale). B) Density of phosphate beads around MTCH2 depicted as orange isosurface wireframe. Lipid phosphates readily insert into the cavity of MTCH2 in both models. In Martini 3, they are also able to easily enter the C-terminal pathway, while this is not the case for Martini 2. The position of the "hydrophobic gate" is indicated by the red arrow. C) Density of water beads around MTCH2 depicted as blue isosurface wireframe. In both models, a large number of molecules of water inserts into the cavity of MTCH2. D) Free energy profiles of lipid flip-flop in a protein-free POPC membrane (black) and along the MTCH2 scrambling pathway (red, blue, and purple). In both models, the presence of MTCH2 dramatically reduces the flip-flop free energy barrier. The red arrow in the Martini 2 chart indicates a peak in the free energy profile corresponding to the "hydrophobic gate". The calculation error is < 1 kJ mol^{-1}.

"credit card mechanism" of lipid scrambling, which involves the lipid head contacting a hydrophilic groove of the protein while the lipid tails face the hydrophobic core of the membrane[14].

To provide a more quantitative picture of the scrambling activity of MTCH2, we calculated the free energy of the entire flip-flop process along the identified scrambling pathway. As shown in Figure 2 D Left, the presence of MTCH2 dramatically decreased the free energy barrier for lipid flip-flop by almost 90% compared to flip-flop in pure POPC bilayer (from 62 to just 7 kJ mol^{-1}).

As Martini 3 may underestimate the free energy barrier for the flip-flop process and consequently overestimate the flip-flop rate, we also performed the same simulations using the older Martini 2.2 force field[2,10,11]. Despite observing a high tendency of lipids and water to enter the cavity of MTCH2, we only observed a handful of complete flip-flop events within the simulated timescale (Figure 2 A Right) likely due to the hindrance of the "hydrophobic gate" described above. Based on these results, we speculate that the opening and closing of the "hydropho-

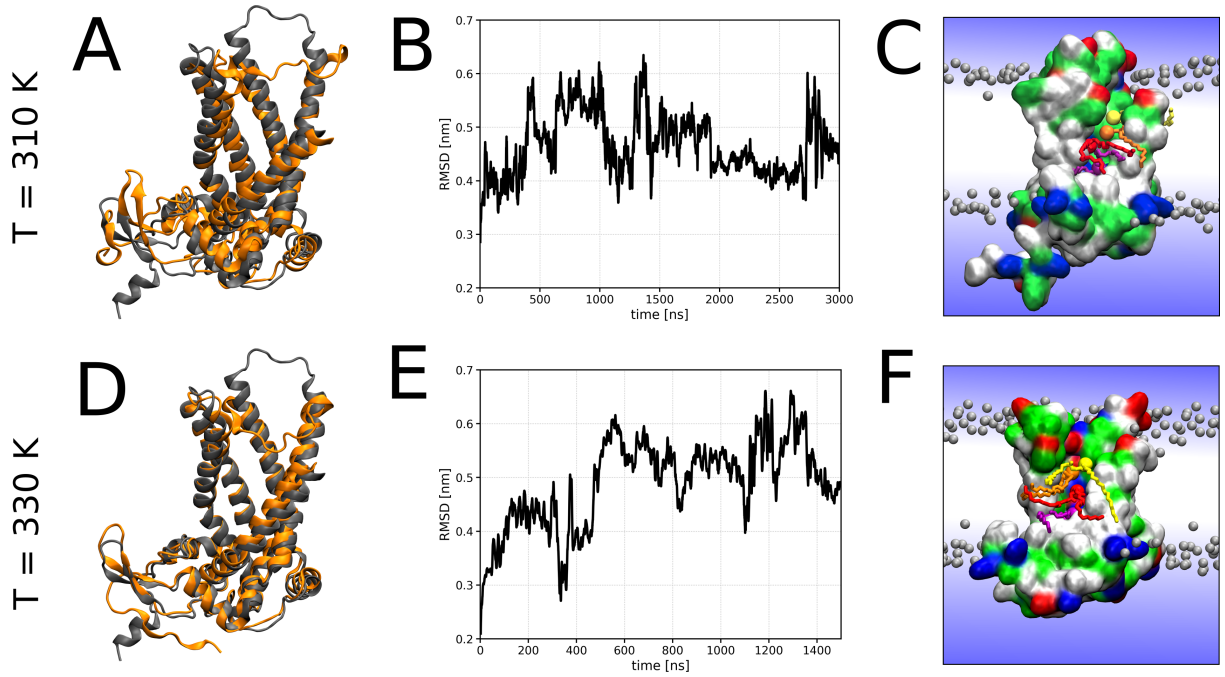

Figure 3: Results of atomistic MD simulations. The upper row (A–C) corresponds to MTCH2 simulated at 310 K, while the lower row (D–F) corresponds to MTCH2 simulated at 330 K. A and D) Cartoon structure of MTCH2 at the start of the simulation (in gray) overlaid with the structure of MTCH2 at the end of the 3 µs (A) or 1.5 µs (D) atomistic simulation (in orange). Note that the α-helical segments of the protein were quite stable and they did not significantly reorient or reposition during either of the simulations. This suggests that the predicted structure is stable and the protein cavity and the scrambling pathway remain open. B and E) Root-mean-square deviation (RMSD) of the MTCH2 backbone during the simulation. Note that while the RMSD fluctuates, it does not systematically increase indicating that the structure is in equilibrium. C and F) Simulation snapshots showing several lipids (colored in yellow, orange, red, and purple) translocating along the scrambling pathway of MTCH2. The protein is shown as a molecular surface colored according to the character of its residues (hydrophilic = green, hydrophobic = white, positively charged = blue, negatively charged = red). Bulk lipids are depicted as gray beads (phosphate group) with hydrophobic tails omitted for clarity. Water is represented only schematically as a blue gradient, omitting the presence of water in the cavity of the protein for visual clarity.

bic gate" could regulate the scrambling activity of MTCH2.

As with Martini 3, we calculated the density of phosphates (Figure 2 B Right) and water (Figure 2 C Right) around MTCH2 showing the tendency of both phosphates and water to enter the cavity of the protein as well as the inability of phosphates to finish the C-terminal part of the scrambling pathway.

Nonetheless, as seen from the calculated free energy profiles (Figure 2 D Right), the presence of MTCH2 still decreases the free energy barrier of the flip-flop process by about 80% compared to the protein-free membrane (from 83 to 15 kJ mol^{-1}).

We acknowledge that the MTCH2 structure predicted by AlphaFold may have some limitations. For instance, the stability of the structure in the membrane may change and the predicted cavity could collapse or only open under specific conditions. The Martini coarse-grained models keep the secondary and tertiary structure of MTCH2 restrained, thereby limiting their dynamics and preventing us from evaluating the stability of the predicted structure. To address this limitation, we simulated MTCH2 using the atomistic CHARMM36m force field[4] in a POPC membrane. In a 3 µs simulation at

physiological conditions, we observed no significant changes in the structure apart from repositioning of the loops (Figure 3 A, B), suggesting the stability of the predicted structure. To further validate this, we performed an additional 1.5 µs simulation of MTCH2 at 330 K (57 °C), which should increase susceptibility to structural alterations. Our observations indicate that the predicted structure is stable and the cavity remains accessible to lipids and water.

The atomistic simulations also indicated a higher likelihood of lipids and water entering the MTCH2 cavity, as illustrated in Figure 3 C. However, we did not observe any full flip-flop event, possibly due to the presence of the "hydrophobic gate" obstructing the lipids from traversing the entire hydrophilic pathway and limited simulation time.

In our Martini 3 simulations, we have observed that MTCH2 displays a scrambling rate similar to that of the VDAC1 dimer, a recently identified scramblase with a beta-barrel structure[5]. The free energy barriers governing lipid flip-flop in the presence of MTCH2 and a VDAC1 dimer are also closely aligned, with values around 7 kJ mol^{-1} according to the Martini 3 model. Notably, both VDAC and MTCH2 are positioned within the outer mitochondrial membrane (OMM), suggesting that MTCH2 could serve as an alternative pathway for lipid scrambling within the OMM. This process is vital for mitochondrial membrane biogenesis and the synthesis of lipids like cardiolipin. However, note that while VDAC requires dimer formation for its scrambling activity, MTCH2 accomplishes lipid scrambling as a monomer, but could be regulated by interacting with other proteins.

In summary, our multiple molecular dynamics simulations and free energy calculations provide evidence for the potential scrambling activity of MTCH2. Starting from the structure predicted by AlphaFold[6], we identified a hydrophilic scrambling pathway that shares structural similarities with other known scramblases. Both our coarse-grained and atomistic simulations consistently show the ability of lipids to enter the membrane core along MTCH2. Moreover, our coarse-grained free energy calculations demonstrate that MTCH2 significantly reduces the free energy barrier for lipid flip-flop. Martini 3 simulations have even resulted in complete lipid flip-flop in both directions along MTCH2, indicating high scrambling activity of this protein. The scrambling rate of MTCH2 is similar to that seen with VDAC dimers[5], which were demonstrated to provide an important mechanism for transfering lipids across the outer membrane of mitochondria. MTCH2 could act redundantly with VDAC, providing complementary scramblase activity. In general, our computational results suggest that insertases such as MTCH2, which possess a hydrophilic path across the membrane, also function as scramblases.

Acknowledgement This work was supported by the National Institutes of Health grant NS119779 (AKM), the European Research Council (ERC) under the European Union's Horizon 2020 research and innovation programme (grant agreement No 101001470) (RV) and the project National Institute of virology and bacteriology (Programme EXCELES, ID Project No. LX22NPO5103) - Funded by the European Union - Next Generation EU (RV). Computational resources were provided by the CESNET, CERIT Scientific Cloud, and IT4 Innovations National Supercomputing Center by MEYS CR through the e-INFRA CZ (ID:90254). We acknowledge the use of the ChatGPT tool in rephrasing the article.

Supporting Information Available

The Supporting Information including extended description of methods and Tables S1-S4 is available free of charge on the ACS Publications website at DOI:

References

(1) Janine D. Brunner, Novandy K. Lim, Stephan Schenck, Alessia Duerst, and Raimund Dutzler. X-ray structure of a

calcium-activated TMEM16 lipid scramblase. *Nature*, 516(7530):207–212, December 2014.

(2) Djurre H. de Jong, Gurpreet Singh, W. F. Drew Bennett, Clement Arnarez, Tsjerk A. Wassenaar, Lars V. Schäfer, Xavier Periole, D. Peter Tieleman, and Siewert J. Marrink. Improved Parameters for the Martini Coarse-Grained Protein Force Field. *Journal of Chemical Theory and Computation*, 9(1):687–697, January 2013.

(3) Alina Guna, Taylor A. Stevens, Alison J. Inglis, Joseph M. Replogle, Theodore K. Esantsi, Gayathri Muthukumar, Kelly C. L. Shaffer, Maxine L. Wang, Angela N. Pogson, Jeff J. Jones, Brett Lomenick, Tsui-Fen Chou, Jonathan S. Weissman, and Rebecca M. Voorhees. MTCH2 is a mitochondrial outer membrane protein insertase. *Science*, 378(6617):317–322, October 2022.

(4) Jing Huang, Sarah Rauscher, Grzegorz Nawrocki, Ting Ran, Michael Feig, Bert L de Groot, Helmut Grubmüller, and Alexander D MacKerell. CHARMM36m: an improved force field for folded and intrinsically disordered proteins. *Nature Methods*, 14(1):71–73, January 2017.

(5) Helene Jahn, Ladislav Bartoš, Grace I Dearden, Jeremy S Dittman, Joost C M Holthuis, Robert Vácha, and Anant K Menon. Phospholipids are imported into mitochondria by vdac, a dimeric beta barrel scramblase. *bioRxiv*, 2023.

(6) John Jumper, Richard Evans, Alexander Pritzel, Tim Green, Michael Figurnov, Olaf Ronneberger, Kathryn Tunyasuvunakool, Russ Bates, Augustin Žídek, Anna Potapenko, Alex Bridgland, Clemens Meyer, Simon A. A. Kohl, Andrew J. Ballard, Andrew Cowie, Bernardino Romera-Paredes, Stanislav Nikolov, Rishub Jain, Jonas Adler, Trevor Back, Stig Petersen, David Reiman, Ellen Clancy, Michal Zielinski, Martin Steinegger, Michalina Pacholska, Tamas Berghammer, Sebastian Bodenstein, David Silver, Oriol Vinyals, Andrew W. Senior, Koray Kavukcuoglu, Pushmeet Kohli, and Demis Hassabis. Highly accurate protein structure prediction with AlphaFold. *Nature*, 596(7873):583–589, August 2021.

(7) Valeria Kalienkova, Vanessa Clerico Mosina, and Cristina Paulino. The Groovy TMEM16 Family: Molecular Mechanisms of Lipid Scrambling and Ion Conduction. *Journal of Molecular Biology*, 433(16):166941, August 2021.

(8) George Khelashvili and Anant K. Menon. Phospholipid Scrambling by G Protein–Coupled Receptors. *Annual Review of Biophysics*, 51(1), May 2022.

(9) Büsra Kizmaz and Johannes M. Herrmann. Membrane insertases at a glance. *Journal of Cell Science*, 136(13):jcs261219, 07 2023.

(10) Siewert J. Marrink, H. Jelger Risselada, Serge Yefimov, D. Peter Tieleman, and Alex H. de Vries. The MARTINI force field: coarse grained model for biomolecular simulations. *The Journal of Physical Chemistry B*, 111(27):7812–7824, jul 2007.

(11) Luca Monticelli, Senthil K. Kandasamy, Xavier Periole, Ronald G. Larson, D. Peter Tieleman, and Siewert-Jan Marrink. The MARTINI coarse-grained force field: Extension to proteins. *Journal of Chemical Theory and Computation*, 4(5):819–834, apr 2008.

(12) Giulia Morra, Asghar M. Razavi, Kalpana Pandey, Harel Weinstein, Anant K. Menon, and George Khelashvili. Mechanisms of Lipid Scrambling by the G Protein-Coupled Receptor Opsin. *Structure*, 26(2):356–367.e3, February 2018.

(13) Fumiya Okawa, Yutaro Hama, Sidi Zhang, Hideaki Morishita, Hayashi Yamamoto, Tim P. Levine, and Noboru Mizushima. Evolution and insights into the structure

and function of the DedA superfamily containing TMEM41B and VMP1. *Journal of Cell Science*, 134(8):jcs255877, April 2021.

(14) T. Pomorski and A. K. Menon. Lipid flippases and their biological functions. *Cellular and Molecular Life Sciences CMLS*, 63(24):2908–2921, 2006.

(15) Takaharu Sakuragi and Shigekazu Nagata. Regulation of phospholipid distribution in the lipid bilayer by flippases and scramblases. *Nature Reviews Molecular Cell Biology*, 24(8):576–596, 2023.

(16) Paulo C. T. Souza, Riccardo Alessandri, Jonathan Barnoud, Sebastian Thallmair, Ignacio Faustino, Fabian Grünewald, Ilias Patmanidis, Haleh Abdizadeh, Bart M. H. Bruininks, Tsjerk A. Wassenaar, Peter C. Kroon, Josef Melcr, Vincent Nieto, Valentina Corradi, Hanif M. Khan, Jan Domański, Matti Javanainen, Hector Martinez-Seara, Nathalie Reuter, Robert B. Best, Ilpo Vattulainen, Luca Monticelli, Xavier Periole, D. Peter Tieleman, Alex H. de Vries, and Siewert J. Marrink. Martini 3: a general purpose force field for coarse-grained molecular dynamics. *Nature Methods*, 18(4):382–388, April 2021.

(17) Mihaly Varadi, Stephen Anyango, Mandar Deshpande, Sreenath Nair, Cindy Natassia, Galabina Yordanova, David Yuan, Oana Stroe, Gemma Wood, Agata Laydon, Augustin Žídek, Tim Green, Kathryn Tunyasuvunakool, Stig Petersen, John Jumper, Ellen Clancy, Richard Green, Ankur Vora, Mira Lutfi, Michael Figurnov, Andrew Cowie, Nicole Hobbs, Pushmeet Kohli, Gerard Kleywegt, Ewan Birney, Demis Hassabis, and Sameer Velankar. AlphaFold Protein Structure Database: massively expanding the structural coverage of protein-sequence space with high-accuracy models. *Nucleic Acids Research*, 50(D1):D439–D444, January 2022.

(18) Yicheng Wang, Anant K. Menon, Yuta Maki, Yi-Shi Liu, Yugo Iwasaki, Morihisa Fujita, Paula A. Guerrero, Daniel Varó'n Silva, Peter H. Seeberger, Yoshiko Murakami, and Taroh Kinoshita. Genome-wide crispr screen reveals clptm1l as a lipid scramblase required for efficient glycosylphosphatidylinositol biosynthesis. *Proceedings of the National Academy of Sciences*, 119(14):e2115083119, 2022.

Supporting Information

Insertases Scramble Lipids: Molecular Simulations of MTCH2

Ladislav Bartoš,[†,‡] Anant K. Menon,[§] and Robert Vácha[*,†,‡,¶]

[†] CEITEC – Central European Institute of Technology, Masaryk University, Kamenice 753/5, 625 00 Brno, Czech Republic
[‡] National Centre for Biomolecular Research, Faculty of Science, Masaryk University, Kamenice 753/5, 625 00 Brno, Czech Republic
[§] Department of Biochemistry, Weill Cornell Medical College, New York, NY 10065, USA
[¶] Department of Condensed Matter Physics, Faculty of Science, Masaryk University, Kotlářská 267/2, 611 37 Brno, Czech Republic
[*] E-mail: robert.vacha@muni.cz

Methods

All molecular dynamics (MD) simulations were performed using the simulation package Gromacs version 2021.4[1] with Plumed plugin version 2.7[24]. The structure of MTCH2 was obtained from the AlphaFold Protein Structure Database (entry Q9Y6C9)[11,25]. Prior to all simulations, the obtained structure of MTCH2 was minimized in vacuum using the Amber 99SB-ILDN force field[13] and the steepest descent algorithm with maximum force tolerance of 100 kJ mol^{-1} nm^{-1}.

Martini simulations

We employed two different versions of the Martini force field: Martini version 3[20] and Martini version 2.2[4,14,15] with ElNeDyn network[18]. The minimized atomistic structure of MTCH2 was coarse-grained using `martinize2` script (available from github.com/marrink-lab/vermouth-martinize) and placed into 1-palmitoyl-2-oleoyl-sn-glycero-3-phosphocholine (POPC) membrane using either `insane` script (Martini 3; available from github.com/Tsjerk/Insane) or CHARMM-GUI (Martini 2)[10]. In Martini 2, the tertiary structure of MTCH2 was maintained using the ElNeDyn network, while in Martini 3, we used elastic network with a force constant of 1000 kJ mol^{-1} nm^{-2} to fix the tertiary structure of the protein.

Each Martini system contained one molecule of MTCH2, roughly 920 POPC lipids, about 19,000 water beads and physiological concentration (0.154 mol dm^{-3}) of NaCl ions (with an excess of ions to neutralize the system). The steepest-descent algorithm was used to minimize each system with a maximum force tolerance of 1000 kJ mol^{-1} nm^{-1}. The equilibration of the systems was performed in five stages, each with different simulation lengths and time steps. The stages were as follows: I) dt = 2 fs, t = 0.5 ns, II) dt = 5 fs, t = 1.25 ns, III) dt = 10 fs, t = 1 ns, IV) dt = 20 fs, t = 30 ns, V) dt = 20 fs, t = 200 ns. During stages I-IV, the Berendsen barostat[2] was utilized, whereas the Parrinello-Rahman barostat[16,17] was used in stage V and in all subsequent simulations. Throughout stages I-IV, a harmonic potential with a force constant of 1000 kJ mol^{-1} nm^{-2} was used to restrain all backbone beads of the MTCH2 protein to their initial positions.

We also constructed one proteinless membrane system for each employed Martini force field as a reference. These systems were smaller, composed of roughly 290 POPC lipids, 6000 water beads, and NaCl ions at physiological concentration. The systems were built using `insane` or CHARMM-GUI (Martini 3 or Martini 2, respectively) and then minimized and equilibrated in the same way as MTCH2 systems, except the stage V of equilibration was shortened to 100 ns. As no protein was present in these systems, no position restraints were applied during the equilibration. The equilibrated structure was then used to perform pulling and subsequently umbrella sampling simulations to obtain the free energy profile of lipid flip-flop in proteinless membrane.

All simulations were performed in the NPT ensemble, with the temperature being maintained at 310 K using stochastic velocity rescaling thermostat[3] with a coupling constant of 1 ps. Water with ions, membrane, and protein were coupled to three separate thermal baths. Pressure was kept at 1 bar using either the Berendsen[2] or Parrinello-Rahman barostat[16,17] (see above) with a coupling constant of 12 ps. Semi-isotropic pressure coupling was used to independently scale the simulation box in the xy-plane and on the z-axis with a compressibility of 3×10^{-4} bar^{-1}. The equations of motion were integrated using the leap-frog algorithm. Non-bonded interactions were cut off at 1.1 nm, and the van der Waals potential was shifted to zero at the cut-off distance. The relative dielectric constant was set to 15 and LINCS[7] parameters `lincs-order` and `lincs-iter` were set to 8 and 2, respectively, to avoid artificial temperature gradients[21].

Three independent molecular dynamics simulations, each 10 µs long, were run from the equilibrated structure of MTCH2-containing membrane for each of Martini 2 and Martini 3 force fields. Every 10 ns, a simulation snapshot was analyzed to determine the percentage of scrambled lipids over time. A lipid was deemed "scrambled" if it was found in a different membrane leaflet than where it began in the simulation, determined by the position of its phosphate bead in relation to the membrane center. The code for analyzing lipid scrambling is available from github.com/ladme/scramblyzer.

For the calculation of water and phosphates densities, all three replicas were merged and centered on protein beads based on their root-mean-square deviation. The densities were calculated using VMD Volmap Tool[9], analyzing a simulation snapshot every 10 ns.

For each of Martini 2 and Martini 3, we calculated the free energy of lipid flip-flop in a) pure POPC membrane and b) in membrane containing MTCH2. Umbrella sampling method[22,23] was used to enhance the sampling of flip-flop events by employing a one-dimensional collective variable (CV). The CV was defined as the oriented distance between the selected lipid phosphate and the local membrane center of mass on the z-axis. The local membrane center of mass was calculated from the positions of lipid beads within a cylinder with a radius of 2.0 nm (for proteinless membrane) or 3.0 nm (for MTCH2 simulations) and its principal axis going through the selected phosphate bead.

Initial configurations for umbrella sampling were generated by pulling the selected lipid phosphate bead through the membrane for 1 µs with a pulling rate of 4.6 nm µs^{-1} (for proteinless membrane) or 4.2 nm µs^{-1} (for MTCH2 simulations) and initial reference distance of 2.3 nm (for proteinless membrane) or ±2.1 nm (for MTCH2 simulations) using a harmonic potential. For systems with MTCH2, we performed two independent pulling simulations. In one pulling simulation, selected lipid was pulled from the upper to the lower membrane leaflet, while in the other pulling simulation, the lipid was pulled in the opposite direction.

44 (Martini 3 simulations with MTCH2), 57 (Martini 2 simulations with MTCH2), or 67 (simulations of proteinless membrane) umbrella sampling windows distributed along the range of the CV were used. In case of MTCH2 simulations, we generated 44 or 57 windows from pulling simulations performed in each direction. As we observed no hysteresis for Martini 3 simulations with MTCH2, we show both of the calculated free energy profiles. In contrast, Martini 2 simulations with MTCH2 did show a hysteresis resulting in a necessity to generate a new set of 57 umbrella sampling windows which initial configurations were obtained from *both* pulling directions. This

umbrella sampling simulation was further enhanced by applying Hamiltonian replica exchange[6] to all the windows with an exchange being attempted every 10,000 simulation steps (200 ps). For Martini 2 simulations with MTCH2, we thus only show one free energy profile.

See the Tables S1–S3 for the complete list of umbrella sampling windows that were used for the calculations. Each window was simulated for 4 µs (Martini 3 simulations with MTCH2), 3 µs (Martini 2 simulations with MTCH2), or 1 µs (proteinless membrane) with the first 10 ns of simulation time being used for equilibration only. In pulling and umbrella sampling simulations with MTCH2, the selected lipid phosphate was restrained to the backbone bead of F228 using a flat-bottom potential with a reference distance of 2.5 nm in the xy plane and a force constant of 500 kJ mol^{-1} nm^{-2}. The translocating lipid was thus effectively restrained to the scrambling pathway, allowing it to sample the relevant portion of the configuration space.

Free energy profiles were obtained using the weighted histogram analysis method[12,19] as implemented in Grossfield Lab WHAM program (available from membrane.urmc.rochester.edu).

Atomistic simulations

For atomistic simulations, we employed the CHARMM36m force field[8]. The MTCH2 structure minimized in vacuum was placed into a POPC membrane using CHARMM-GUI[10]. The system contained one protein, roughly 390 lipid molecules, 37,000 molecules of water, and NaCl ions at a concentration of 0.154 mol dm^{-3} (with an excess of ions to neutralize the system). Minimization was performed using the steepest-descent algorithm and force tolerance of 1000 kJ mol^{-1} nm^{-1}. During the minimization, positions restraints were applied to protein backbone and protein sidechains (force constant of 4000 and 2000 kJ mol^{-1} nm^{-2}, respectively) as well as to phosphorus atom of each lipid (force constant of 1000 kJ mol^{-1} nm^{-2}). Dihedral restraints (force constant of 1000 kJ mol^{-1} rad^{-2}) were further applied to two dihedral angles in all POPC molecules, specifically to dihedrals between C1, C3, C2, and O21 (glycerol carbons and oxygen linking the oleoyl tail to glycerol) and between C28, C29, C210, and C211 (carbons around the double bond of the oleyol tail), fixing them at $-120° \pm 2.5°$ and $0° \pm 0.0°$, respectively.

Equilibration was performed in 6 stages of different simulation lengths: I-III) 250 ps (each), IV-V) 1 ns, VI) 5 ns. Stages I-II were performed in the NVT ensemble, while stages III-VI in the NPT ensemble. Stochastic velocity rescaling thermostat[3] with a coupling constant of 0.5 ps was employed to maintain the temperature of 310 K. Three separate thermal baths were used for water with ions, membrane, and protein. In NPT stages of equilibration, pressure was kept at 1 bar using the Berendsen barostat[2] with semi-isotropic pressure coupling, coupling constant of 5 ps and compressibility of 4.5×10^{-5} bar^{-1}. The equations of motion were integrated using the leap-frog algorithm. In stages I-III, the simulation time step was 1 fs, while in the rest of the equilibration (and the following simulations), the time step was 2 fs. Short-ranged non-bonded interactions were truncated at 1.2 nm, while a force switch was applied starting from 1.0 nm. Electrostatic interactions were treated using Fast smooth Particle-Mesh Ewald[5]. Bonds with hydrogens were constrained using the LINCS algorithm[7]. Translational velocity removal was applied separately for membrane with protein and for water with ions. Position and dihedral restraints were strong in the initial stages of equilibration and then gradually turned down, see Table S4.

After equilibration, we performed 3 µs long production simulation. In this simulation, the Berendsen thermostat was replaced with Parrinello-Rahman barostat[16,17] and no restraints were applied to the system. All the other simulation settings remained the same as in the stage VI of equilibration. RMSD of protein backbone atoms was calculated using the Gromacs `rms` tool.

We also performed a simulation in which the MTCH2 protein was heated up to further assess its thermodynamic stability. Starting from the minimized structure of the system, we performed a new equilibration with the same simulation settings except the temperature of the protein was

increased to 330 K. The same temperature was also applied in the following 1.5 µs long production simulation. The temperature of the membrane and water with ions was kept at the physiological 310 K.

Table S1: Distribution of umbrella sampling windows along the collective variable with biasing force constants used for Martini 3 simulations of lipid flip-flop through membrane with MTCH2. Reference distances are in nm, force constants in kJ mol^{-1} nm^{-2}.

Reference distance	Force constant	Reference distance	Force constant
2.00	100	−0.50	200
1.80	100	−0.60	200
1.60	100	−0.70	200
1.40	100	−0.80	200
1.30	200	−0.85	400
1.20	200	−0.90	400
1.10	200	−0.95	400
1.00	200	−1.00	400
0.90	200	−1.05	400
0.80	200	−1.10	400
0.70	200	−1.15	400
0.60	200	−1.20	400
0.50	200	−1.25	400
0.40	200	−1.30	400
0.30	200	−1.40	200
0.20	200	−1.50	200
0.10	200	−1.60	200
0.00	200	−1.70	200
−0.10	200	−1.80	200
−0.20	200	−1.90	200
−0.30	200	−2.00	100
−0.40	200	−2.10	100

Table S2: Distribution of umbrella sampling windows along the collective variable with biasing force constants used for Martini 2 simulations of lipid flip-flip through membrane with MTCH2. Reference distances are in nm, force constants in kJ mol^{-1} nm^{-2}.

Reference distance	Force constant	Reference distance	Force constant
2.10	300	−0.80	500
2.00	300	−0.85	2000
1.90	500	−0.90	2000
1.80	500	−0.95	3000
1.70	500	−1.00	3000
1.60	500	−1.04	5000
1.50	500	−1.06	5000
1.40	500	−1.08	5000
1.30	500	−1.10	5000
1.20	500	−1.12	5000
1.10	500	−1.14	5000
1.00	500	−1.16	5000
0.90	500	−1.18	5000
0.80	500	−1.20	5000
0.70	500	−1.22	5000
0.60	500	−1.25	3000
0.50	500	−1.30	3000
0.40	500	−1.35	2000
0.30	500	−1.40	2000
0.20	500	−1.45	500
0.10	500	−1.50	500
0.00	500	−1.60	500
−0.10	500	−1.70	500
−0.20	500	−1.80	500
−0.30	500	−1.90	500
−0.40	500	−2.00	300
−0.50	500	−2.10	300
−0.60	500	−2.20	300
−0.70	500		

Table S3: Distribution of umbrella sampling windows along the collective variable with biasing force constants used for Martini 2 and 3 simulations of lipid flip-flop through proteinless membrane. Reference distances are in nm, force constants in kJ mol^{-1} nm^{-2}.

Reference distance	Force constant	Reference distance	Force constant
2.30	1000	−0.05	4000
2.20	1000	−0.10	4000
2.10	1000	−0.15	3000
2.00	1000	−0.20	3000
1.90	1000	−0.25	3000
1.80	1000	−0.30	3000
1.70	1000	−0.35	2000
1.60	1000	−0.40	2000
1.50	1000	−0.45	2000
1.40	1000	−0.50	2000
1.30	1000	−0.55	2000
1.20	1000	−0.60	2000
1.10	1000	−0.65	2000
1.00	2000	−0.70	2000
0.95	2000	−0.75	2000
0.90	2000	−0.80	2000
0.85	2000	−0.85	2000
0.80	2000	−0.90	2000
0.75	2000	−0.95	2000
0.70	2000	−1.00	2000
0.65	2000	−1.10	1000
0.60	2000	−1.20	1000
0.55	2000	−1.30	1000
0.50	2000	−1.40	1000
0.45	2000	−1.50	1000
0.40	2000	−1.60	1000
0.35	2000	−1.70	1000
0.30	2000	−1.80	1000
0.25	3000	−1.90	1000
0.20	3000	−2.00	1000
0.15	3000	−2.10	1000
0.10	4000	−2.20	1000
0.05	4000	−2.30	1000
0.00	4000		

Table S4: Position and dihedral restraints applied during the individual stages of atomistic equilibration. All values are in kJ mol^{-1} nm^{-2} or kJ mol^{-1} rad^{-2} (for lipid dihedrals).

	protein backbone	protein sidechains	lipid phosphorus	lipid dihedrals
I	4000	2000	1000	1000
II	2000	1000	400	400
III	1000	500	400	200
IV	500	200	200	200
V	200	50	40	100
VI	50	0	0	0

References

(1) Mark James Abraham, Teemu Murtola, Roland Schulz, Szilárd Páll, Jeremy C. Smith, Berk Hess, and Erik Lindahl. GROMACS: High performance molecular simulations through multi-level parallelism from laptops to supercomputers. *SoftwareX*, 1-2:19–25, September 2015.

(2) H. J. C. Berendsen, J. P. M. Postma, W. F. van Gunsteren, A. DiNola, and J. R. Haak. Molecular dynamics with coupling to an external bath. *The Journal of Chemical Physics*, 81(8):3684–3690, October 1984.

(3) Giovanni Bussi, Davide Donadio, and Michele Parrinello. Canonical sampling through velocity rescaling. *The Journal of Chemical Physics*, 126(1):014101, jan 2007.

(4) Djurre H. de Jong, Gurpreet Singh, W. F. Drew Bennett, Clement Arnarez, Tsjerk A. Wassenaar, Lars V. Schäfer, Xavier Periole, D. Peter Tieleman, and Siewert J. Marrink. Improved Parameters for the Martini Coarse-Grained Protein Force Field. *Journal of Chemical Theory and Computation*, 9(1):687–697, January 2013.

(5) Ulrich Essmann, Lalith Perera, Max L. Berkowitz, Tom Darden, Hsing Lee, and Lee G. Pedersen. A smooth particle mesh Ewald method. *The Journal of Chemical Physics*, 103(19):8577–8593, November 1995.

(6) Hiroaki Fukunishi, Osamu Watanabe, and Shoji Takada. On the hamiltonian replica exchange method for efficient sampling of biomolecular systems: Application to protein structure prediction. *The Journal of Chemical Physics*, 116(20):9058–9067, 2002.

(7) Berk Hess, Henk Bekker, Herman J. C. Berendsen, and Johannes G. E. M. Fraaije. LINCS: A linear constraint solver for molecular simulations. *Journal of Computational Chemistry*, 18(12):1463–1472, September 1997.

(8) Jing Huang, Sarah Rauscher, Grzegorz Nawrocki, Ting Ran, Michael Feig, Bert L de Groot, Helmut Grubmüller, and Alexander D MacKerell. CHARMM36m: an improved force field for folded and intrinsically disordered proteins. *Nature Methods*, 14(1):71–73, January 2017.

(9) William Humphrey, Andrew Dalke, and Klaus Schulten. VMD – Visual Molecular Dynamics. *Journal of Molecular Graphics*, 14:33–38, 1996.

(10) Sunhwan Jo, Taehoon Kim, Vidyashankara G. Iyer, and Wonpil Im. CHARMM-GUI: A web-based graphical user interface for CHARMM. *Journal of Computational Chemistry*, 29(11):1859–1865, mar 2008.

(11) John Jumper, Richard Evans, Alexander Pritzel, Tim Green, Michael Figurnov, Olaf Ronneberger, Kathryn Tunyasuvunakool, Russ Bates, Augustin Žídek, Anna Potapenko, Alex Bridgland, Clemens Meyer, Simon A. A. Kohl, Andrew J. Ballard, Andrew Cowie, Bernardino Romera-Paredes, Stanislav Nikolov, Rishub Jain, Jonas Adler, Trevor Back, Stig Petersen, David Reiman, Ellen Clancy, Michal Zielinski, Martin Steinegger, Michalina Pacholska, Tamas Berghammer, Sebastian Bodenstein, David Silver, Oriol Vinyals, Andrew W. Senior, Koray Kavukcuoglu, Pushmeet Kohli, and Demis Hassabis. Highly accurate protein structure prediction with AlphaFold. *Nature*, 596(7873):583–589, August 2021.

(12) Shankar Kumar, John M. Rosenberg, Djamal Bouzida, Robert H. Swendsen, and Peter A. Kollman. The weighted histogram analysis method for free-energy calculations on biomolecules. I. The method. *Journal of Computational Chemistry*, 13(8):1011–1021, October 1992.

(13) Kresten Lindorff-Larsen, Stefano Piana, Kim Palmo, Paul Maragakis, John L. Klepeis, Ron O. Dror, and David E. Shaw. Improved side-chain torsion potentials for the Amber ff99SB protein force field: Improved Protein Side-Chain Potentials. *Proteins: Structure, Function, and Bioinformatics*, 78(8):1950–1958, June 2010.

(14) Siewert J. Marrink, H. Jelger Risselada, Serge Yefimov, D. Peter Tieleman, and Alex H. de Vries. The MARTINI force field: coarse grained model for biomolecular simulations. *The Journal of Physical Chemistry B*, 111(27):7812–7824, jul 2007.

(15) Luca Monticelli, Senthil K. Kandasamy, Xavier Periole, Ronald G. Larson, D. Peter Tieleman, and Siewert-Jan Marrink. The MARTINI coarse-grained force field: Extension to proteins. *Journal of Chemical Theory and Computation*, 4(5):819–834, apr 2008.

(16) M. Parrinello and A. Rahman. Crystal structure and pair potentials: A molecular-dynamics study. *Physical Review Letters*, 45(14):1196–1199, oct 1980.

(17) M. Parrinello and A. Rahman. Polymorphic transitions in single crystals: A new molecular dynamics method. *Journal of Applied Physics*, 52(12):7182–7190, dec 1981.

(18) Xavier Periole, Marco Cavalli, Siewert-Jan Marrink, and Marco A. Ceruso. Combining an Elastic Network With a Coarse-Grained Molecular Force Field: Structure, Dynamics, and Intermolecular Recognition. *Journal of Chemical Theory and Computation*, 5(9):2531–2543, September 2009.

(19) Marc Souaille and Benoit Roux. Extension to the weighted histogram analysis method: combining umbrella sampling with free energy calculations. *Computer Physics Communications*, 135(1):40–57, March 2001.

(20) Paulo C. T. Souza, Riccardo Alessandri, Jonathan Barnoud, Sebastian Thallmair, Ignacio Faustino, Fabian Grünewald, Ilias Patmanidis, Haleh Abdizadeh, Bart M. H. Bruininks, Tsjerk A. Wassenaar, Peter C. Kroon, Josef Melcr, Vincent Nieto, Valentina Corradi, Hanif M. Khan, Jan Domański, Matti Javanainen, Hector Martinez-Seara, Nathalie Reuter, Robert B. Best, Ilpo Vattulainen, Luca Monticelli, Xavier Periole, D. Peter Tieleman, Alex H. de Vries, and Siewert J. Marrink. Martini 3: a general purpose force field for coarse-grained molecular dynamics. *Nature Methods*, 18(4):382–388, April 2021.

(21) Sebastian Thallmair, Matti Javanainen, Balázs Fábián, Hector Martinez-Seara, and Siewert J. Marrink. Nonconverged Constraints Cause Artificial Temperature Gradients in Lipid Bilayer Simulations. *The Journal of Physical Chemistry B*, 125(33):9537–9546, August 2021.

(22) G.M. Torrie and J.P. Valleau. Monte Carlo free energy estimates using non-Boltzmann sampling: Application to the sub-critical Lennard-Jones fluid. *Chemical Physics Letters*, 28(4):578–581, October 1974.

(23) G.M. Torrie and J.P. Valleau. Nonphysical sampling distributions in Monte Carlo free-energy estimation: Umbrella sampling. *Journal of Computational Physics*, 23(2):187–199, February 1977.

(24) Gareth A. Tribello, Massimiliano Bonomi, Davide Branduardi, Carlo Camilloni, and Giovanni Bussi. PLUMED 2: New feathers for an old bird. *Computer Physics Communications*, 185(2):604–613, feb 2014.

(25) Mihaly Varadi, Stephen Anyango, Mandar Deshpande, Sreenath Nair, Cindy Natassia, Galabina Yordanova, David Yuan, Oana Stroe, Gemma Wood, Agata Laydon, Augustin Žídek, Tim Green, Kathryn Tunyasuvunakool, Stig Petersen, John Jumper, Ellen Clancy, Richard Green, Ankur Vora, Mira Lutfi, Michael Figurnov, Andrew Cowie, Nicole Hobbs, Pushmeet Kohli, Gerard Kleywegt, Ewan Birney, Demis Hassabis, and Sameer Velankar. AlphaFold Protein Structure Database: massively expanding the structural coverage of protein-sequence space with high-accuracy models. *Nucleic Acids Research*, 50(D1):D439–D444, January 2022.